

Topological Transitions and Bulk Wavefunctions in the SSH Model

David S. Simon,^{1,2,*} Shuto Osawa,^{2,†} and Alexander V. Sergienko^{2,3,‡}

¹*Dept. of Physics and Astronomy, Stonehill College, 320 Washington Street, Easton, MA 02357*

²*Dept. of Electrical and Computer Engineering & Photonics Center,
Boston University, 8 Saint Mary's St., Boston, MA 02215, USA*

³*Dept. of Physics, Boston University, 590 Commonwealth Ave., Boston, MA 02215, USA*

Working in the context of the Su-Schreiffer-Heeger (SSH) model, the effect of topological transitions on the structure and properties of bulk position-space wavefunctions is studied for a particle undergoing a quantum walk in a one-dimensional lattice. In particular, we consider what happens when the wavefunction reaches a boundary at which the Hamiltonian changes suddenly from one topological phase to another. An exact solution is constructed for the wavefunction on both sides of the boundary. Under some conditions, it is found that the probability of transition into the region of the second, topologically distinct Hamiltonian is strongly suppressed. When the boundary is encountered, the wavefunctions tend to be strongly reflected, and by appropriate choice of system parameters leakage into the second region can be made negligible. Therefore, it is possible to arrange a high degree of bulk wavefunction localization within in each region. This “topologically-assisted” suppression of transitions, although not of direct topological origin itself, exists only because of the presence of a change in the topological properties of the Hamiltonian. We give a quantitative examination of the reflection and transmission coefficients of incident waves at the boundary between regions of different winding number.

I. INTRODUCTION

The Su-Schreiffer-Heeger (SSH) model [1] was originally proposed as a model of electron behavior in polymers, but has become widely used as a simple model in which topological phase transitions may occur. The system is defined in terms of two parameters, w and v , representing hopping amplitudes between two distinct types of lattice sites. Each unit cell is formed by a pair of lattice sites, one of each type (Fig. 1). As the quasimomentum k varies across the full Brillouin zone, the Hamiltonian \hat{H} traces out a closed curve in a two-dimensional space. When the parameters obey $v > w$ this curve avoids enclosing the origin, where \hat{H} becomes singular, and so the Hamiltonian exhibits a vanishing winding number about the singularity [2–4]. For $v < w$, the curve encloses the singular point, and has winding number 1 about the origin. At the borderline case $v = w$, a transition between two topological phases occurs, with the winding number making a discontinuous jump. Since the SSH lattice has two distinct sublattices, corresponding to two “internal states” within each unit cell, the energies form two bands separated by a finite gap. However, when $v = w$, the gap disappears, and at this point transitions between different winding numbers occur.

In treatments of the SSH model, the emphasis is usually on the Hamiltonian and the energy bands. Wavefunctions are normally given less attention, and when they are discussed the focus is usually on Bloch states in momentum space or on the localized edge states that ap-

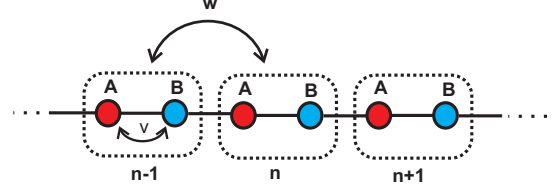


FIG. 1: The SSH Hamiltonian describes motion of a particle hopping on a chain of sites with two substates per site. v and w are respectively the intracell and intercell hopping amplitudes per unit time.

pear between regions of different winding number. However, recently the behavior of particles undergoing quantum walks in SSH-like systems has become an important topic of research; in particular photonic quantum walks in linear optical systems have been shown to simulate topological states of the same type that appear in SSH-like systems [5–11]. In these photonic systems, the particle is inserted at a fixed location, then at a later time (after some number of discrete time steps) its final position distribution is measured. Thus, position-space wavefunctions in the bulk are of significant interest and hold the key to a more complete understanding to transitions between topologically distinct regions.

Figure 2 shows a simulation of a photonic quantum walk. In (a), the entire system has the same Hamiltonian, and the photon spreads ballistically in both directions from the point of insertion, displaying the well-known probability distribution of quantum walk systems. However, in (b) the parameters of the system abruptly change at lattice site 85, causing the Hamiltonian on the right side of that point to have a different winding number than the Hamiltonian to the left. It can be clearly seen that penetration of the photon into the region on the right is

*e-mail: simond@bu.edu

†e-mail: sosawa@bu.edu

‡e-mail: alexserg@bu.edu

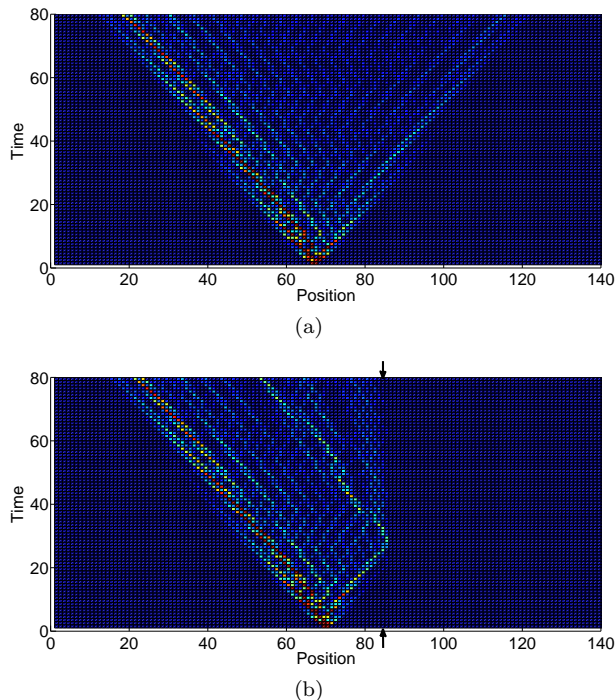


FIG. 2: Calculated probability distribution of detecting a photon at position x at time t as the photon undergoes a one-dimensional quantum walk. The system in which the photon is walking is the linear optical arrangement of [12]. (a) The Hamiltonian is the same (of winding number zero) throughout. The photon is inserted into the system at position $x = 70$ and then exhibits the ballistic evolution characteristic of quantum walks. (b) The same, except that now the parameters of the system change at position $x = 85$ (marked by the arrows) so that the winding number of the Hamiltonian is 0 to the left of that point and 1 to the right. It can be seen that propagation into the region of “wrong” winding number is strongly suppressed.

strongly suppressed, with some of the amplitude collecting at the boundary and most of the rest reflecting back into the original region. Such a suppression of transitions into regions of different winding number may be seen in experimental data as well (see Fig. 3 of [8] for example), although in experiments the effect is somewhat obscured due to the small number of steps measured and the presence of the localized state at the boundary that extends a few steps into the second region. Possibly because of these obscuring factors, this effect has not been much remarked upon. One possible interpretation is simply a mismatch between energy levels on the two sides of the boundary, but it is also possible that *the change in topology plays a role* regardless of the energies. Our goal here is to examine this question more closely.

More specifically, this paper looks in detail at position-space wavefunctions of SSH systems and at what happens to them when the topology of the Hamiltonian changes. We assume that the Hamiltonian depends on some pa-

rameter that is under the control of experimenters (for example, the vertex phase parameters in the quantum walk systems of [11, 12] or the rotation angles of [5–9]). We further assume that the parameter varies in such a way that at some position x it causes the winding number of the Hamiltonian to change. Although all of the considerations in the following sections apply equally to other physical realizations, we will assume for the sake of specificity that the particles involved are photons.

At the boundary between the two regions there should be a transition between states that are asymptotically (far from the boundary) eigenstates of the original Hamiltonian to eigenstates of the topologically-altered Hamiltonian. We show in the following that if the two Hamiltonians are of different winding number, then such transitions are partially suppressed by an amount depending on the values of the v and w parameters of the two Hamiltonians, with strong reflection at the interface. The net result is that in a system of regions governed by Hamiltonians of different winding number, if the hopping amplitudes are well-chosen, then states will strongly tend to remain in the region where they started and resist propagation into other regions. Although we have been speaking of spatial regions here, the same will apply to different regions of some more abstract parameter space: for example if a system is arranged such that photons see a polarization-dependent Hamiltonian that has different winding number for vertical and horizontal cases, then polarization flips will be suppressed by the same mechanism. This has obvious applications, for example in reducing the likelihood of polarization-flip errors in optical information processing systems. It will be shown elsewhere that Hamiltonians with such polarization-dependent winding numbers can be readily engineered using linear optics.

The existence of localized, topologically protected states at the boundaries between regions with different winding number is well-known. The results here imply that under appropriate conditions there is also a measure of “protection” attached to the bulk wavefunctions, in the sense that propagation into spatial regions or parameter regions with different topological properties is suppressed. The degree of transition suppression between these regions depends on the parameter values themselves, as well as the presence or absence of discrete topology changes. In this paper we only examine the simplest case, in which the two hopping parameters are interchanged at the boundary: the value of v on the left equals the value of w on the right, and vice-versa. A quantitative study of how the suppression varies as the values of v and w move away from the pure exchange case will be carried out elsewhere.

Note further that if one can strongly suppress transitions of the bulk wavefunction between regions of parameter space of different topology, one can associate the wavefunction localized in a given region with a Hamiltonian of particular topology. Then linear combinations of states associated to different winding number Hamil-

tonians may be formed, allowing winding number-based qubits. Such linear combinations can be easily arranged, for example, by inserting linear combinations of polarization states, with different polarizations being governed by Hamiltonians of different winding number. These qubits can be thought of as being encoded into either the particle state or the associated Hamiltonian. Gates can then be made that act by altering the Hamiltonian, with read-out accomplished by making measurements on the states.

In the coming sections, we will see that the presence of a change in the topology of the Hamiltonian (a discrete change in its winding number) affects the transmission and reflection coefficients at the boundary point. In the absence of the topology change, the transmission coefficient is uniformly equal to 100%. However, when the topology change is in place the transmission coefficient becomes a continuous function of the hopping parameters, and for some parameter ranges the transmission can be made very small.

This discussion points out that there is interplay between discrete, topologically-based variables (winding number) and continuous variable (transmission coefficient) that may be affected by them. Such interplay exists in many other contexts. Consider, for example, a particle striking a potential barrier of height V_0 from the left. The barrier is discrete: you are either at the top (on the right) or at the bottom (on the left), with no possibility of being in between. The top/bottom distinction only exists because of the discrete jump in potential at the origin. The transmission coefficient for the particle to move from left to right, however, is continuous as a function of energy. Despite being continuous, it depends on the existence of the discrete potential step. When the particle energy E satisfies $E < V_0$ the transmission amplitude t is uniformly zero, but as the energy increases to the point where E exceeds V_0 , t becomes a continuously-varying function of E . So the value of the transmission amplitude is affected by the discrete variable, and yet remains a continuous function of its parameters (energy in this case), and for some parameter values becomes negligible. The situation in our case is directly analogous, with the discrete potential step replaced by a discrete topology change and the transmission amplitude's dependence on the energy replaced by dependence on hopping parameters.

A similar analogy occurs at the edge of a step-index optical fiber. The refractive index changes discretely, but that change affects the properties of the reflected and evanescent waves. Without the discrete jump there would be no evanescent wave at all; but the properties of that wave (penetration depth, etc.) still depend continuously on other parameters such as the angle of incidence.

In this paper, we show that reflections occur at the points of sudden topological changes, in the same manner that reflections occur at any other abrupt change such as a sudden change in potential energy, acoustic impedance, or refractive index. We use the Su-Schreiffer-Heeger (SSH) system as an example system. In many

applications of the SSH model, the electron or other hopping particle is treated as a point particle, perfectly localized at a given lattice site at each moment. In reality, we know that quantum mechanical wavefunctions typically have a finite spread to them and this spread needs to be taken into account to study quantities like scattering amplitudes and tunneling rates. In the current paper we are looking at the transition rate from one side of a discrete boundary to the other side, and this will clearly be dependent on the wave-like properties of the particle. So we focus on the position-space wavefunction and expand it in a convenient basis. In the context of a particle interacting with a discrete lattice system, a convenient basis is the Wannier basis, in which the wavefunction is built out of basis states localized near each lattice site. A particle initially localized near one site will exhibit a quantum walk [4, 13–15], evolving into a superposition of states localized at many sites; what we compute is the rate of transmission of this quantum walk state from one side of a topological boundary to the other.

The plan of the paper is as follows. In Section II we briefly review the SSH model and set up the notation for what follows. In Section III we construct the position- and momentum-space wavefunctions expressed in the Wannier basis. In Section IV we carry out a quantitative examination of reflection and transmission of the wavefunction at the boundary, making use of the transmission coefficient calculated explicitly in the appendix. Finally, we summarize the results and discuss further aspects of them in Section V.

II. BRIEF REVIEW OF SSH MODEL

The Su-Schreiffer-Heeger (SSH) Hamiltonian [1] in one dimension describes the hopping of particles along the length of a bipartite lattice. A closely related model arose independently in quantum field theory [16].

The SSH system is shown schematically in Fig. 1. There is a lattice of unit cells, labeled by integer n , each of which contains two subsites, denoted as A and B ; these subsites represent two possible “internal” states at cell n . There is an amplitude per unit time v to switch between the two states within the same cell, and an amplitude per time w to hop to an adjacent lattice site. Hopping to an adjacent site is always accompanied by a change of the internal state. By redefining the basis states if necessary, the hopping amplitudes v and w can always be chosen, without loss of generality, to be real.

Let R represent lattice positions and r be the position of the particle moving through the lattice. It is convenient to take the center of each unit cell to be at integer-valued positions, $R = n$, for $n = 1, 2, \dots, N$, midway between the A and B subsites, as in Fig. 3. So the spacing between cells is one unit and the spacing between the A and B subsites within a cell is $1/2$ unit. Then the A subsites are at locations $n - \frac{1}{4}$ and the B sites are at $n + \frac{1}{4}$. In order to avoid edge effects, we may take

periodic boundary conditions, so that site $n = N + 1$ is identified with site $n = 1$, or we may simply take N to be very large.

The position-space Hamiltonian is of the form:

$$\hat{H} = v \sum_{n=1}^N (|B, n\rangle\langle A, n| + |A, n\rangle\langle B, n|) + w \sum_{n=1}^{N-1} (|A, n+1\rangle\langle B, n| + |B, n\rangle\langle A, n+1|). \quad (1)$$

Here, $|A, n\rangle$, for example, denotes the state with a particle at site n in substate A .

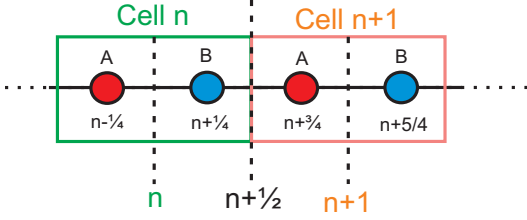


FIG. 3: Two unit cells of the lattice. The coordinates are chosen so that the center of each cell is at an integer-valued location. The two substates A and B are equally distant from the cell's center, so they are separated by half a unit, at locations $n \pm \frac{1}{4}$, for $n = 1, 2, \dots, N$

At each fixed cell n or each fixed momentum k , this Hamiltonian is therefore a two-dimensional matrix, and can be expanded in terms of the identity matrix and the Pauli matrices; for example, in momentum space one may write

$$\hat{H}(k) = d_0(k)I + \mathbf{d}(k) \cdot \boldsymbol{\sigma}. \quad (2)$$

This describes dynamics in a two dimensional “internal” subspace labeled by the two substates present at each lattice site. Generically, the two energy levels are separated by a k -dependent gap.

The Hamiltonian is completely characterized by the 4-dimensional vector $\{d_0(k), \mathbf{d}(k)\}$. In the SSH model $d_0 = d_z = 0$, leaving $\mathbf{d}(k)$ confined to a plane. There is a singular point in this plane, at $\mathbf{d}(k) = 0$, where the phase of the Hamiltonian becomes indeterminate and the energy gap between bands vanishes. As k is varied across a full Brillouin zone, $\mathbf{d}(k)$ traces out a closed curve. These curves can be divided into two distinct classes: those that encircle the singular point and those that don't. In other words, those whose winding number about the origin is $\nu = 1$, and those of winding number $\nu = 0$. The winding number is highly stable in the sense that local perturbations causing continuous variations of the parameters cannot stimulate transitions between the discrete topological classes. Only a strong disturbance that alters the global structure of the system can cause the winding number to change.

In momentum space, the Hamiltonian is block diagonal, with blocks at each k value of the form

$$\hat{H}(k) = \begin{pmatrix} 0 & v + w e^{-ik} \\ v + w e^{+ik} & 0 \end{pmatrix} = \begin{pmatrix} 0 & z \\ z^* & 0 \end{pmatrix}, \quad (3)$$

where $z = v + w e^{-ik}$. The two dimensions of this matrix correspond to the two substates A and B inside the unit cell.

An alternative form of this Hamiltonian will be useful. The off-diagonal terms can be written in polar form in the complex plane:

$$z = v + w e^{-ik} = e^{-ik/2} (v e^{ik/2} + w e^{-ik/2}) \quad (4)$$

$$= e^{-ik/2} \left((v + w) \cos\left(\frac{k}{2}\right) + i(v - w) \sin\left(\frac{k}{2}\right) \right) \quad (5)$$

$$= e^{-ik/2} \left((v + w)^2 \cos^2\left(\frac{k}{2}\right) + (v - w)^2 \sin^2\left(\frac{k}{2}\right) \right)^{1/2} e^{i\theta_k} \quad (6)$$

$$= E_k e^{i\theta_k - ik/2}, \quad (7)$$

where

$$E_k = \left((v + w)^2 \cos^2\left(\frac{k}{2}\right) + (v - w)^2 \sin^2\left(\frac{k}{2}\right) \right)^{1/2} \quad (8)$$

$$= (v^2 + w^2 + 2vw \cos k)^{1/2} \quad (9)$$

is the absolute value of z , while

$$\theta_k = \tan^{-1} \left(\frac{\text{Im}(z)}{\text{Re}(z)} \right) \quad (10)$$

$$= \tan^{-1} \left(\frac{(v - w)}{(v + w)} \tan \frac{k}{2} \right) \quad (11)$$

is the phase. So the Hamiltonian can be written as

$$H(k) = E_k \begin{pmatrix} 0 & e^{i\theta_k - ik/2} \\ e^{-i\theta_k + ik/2} & 0 \end{pmatrix}, \quad (12)$$

showing clearly the winding of H in the complex plane as the angle θ_k changes. The factor $\theta_k - \frac{k}{2}$ in the exponent is, up to a constant, a geometric Berry phase.

The eigenvalues are

$$E_{\pm}(k) = \pm E_k = \pm \sqrt{v^2 + w^2 + 2vw \cos k}. \quad (13)$$

It is then easy to verify that the eigenvectors are (up to an arbitrary overall phase):

$$|\pm\rangle = \frac{1}{\sqrt{2}} \begin{pmatrix} 1 \\ \pm e^{-i(\theta_k - \frac{k}{2})} \end{pmatrix} \equiv \frac{1}{\sqrt{2}} \begin{pmatrix} u_{\pm} \\ l_{\pm} \end{pmatrix}. \quad (14)$$

The upper component corresponds to the A substate, the lower to the B substate.

It should be kept in mind that the quasi-momentum k and the quasi-energy E are only defined modulo 2π .

III. POSITION-SPACE WAVEFUNCTIONS

Ignoring for the moment the A and B subcells, consider a simple lattice with N sites at positions $R = 1, 2, \dots, N$. One may construct the one-dimensional Bloch wavefunctions for particle propagating through the lattice,

$$\psi_k(r) = e^{ikr} u_k(r), \quad (15)$$

where r is the particle position, and the allowed momenta are

$$k_n = \frac{2\pi n}{N} - \pi, \quad (16)$$

with $n = 1, \dots, N$. We take the first Brillouin zone to run over the interval $-\pi < k \leq +\pi$. For a single k value, the corresponding position space wavefunction can be written in terms of the Wannier functions $\phi_R(r) = \phi(r - R)$ [17–19]:

$$u_k(r) = \frac{1}{\sqrt{N}} \sum_R e^{-ik(r-R)} \phi(r - R) \quad (17)$$

$$\psi_k(r) = e^{ikr} u_k(r) = \frac{1}{\sqrt{N}} \sum_R e^{ikR} \phi(r - R). \quad (18)$$

Wannier functions are widely used in solid state physics and other areas, and are defined as the Fourier transforms of the Bloch wavefunctions with respect to the discrete lattice positions,

$$\phi_R(r) = \phi(r - R) = \frac{1}{\sqrt{N}} \sum_k e^{-ikR} \psi_k(r). \quad (19)$$

There is one such function for each point in the crystal lattice and they are strongly localized near those lattice sites.

The functions centered at different lattice sites are orthogonal,

$$\int \phi^*(r - R) \phi(r - R') dr = \delta(R - R'), \quad (20)$$

so the Wannier functions form a complete basis for spatial wavefunctions on the lattice. For the SSH model, these get multiplied by a two-dimensional column matrix in the internal A/B space spanned by the two subsites at each n .

Now introduce the A and B sublattices, so that the lattice sites are shifted to $R = n \pm \frac{1}{4}$, where $n = 1, 2, \dots, N$. This splits each term in the sum of Eq. 15 into two terms, one shifted the left by $\frac{1}{4}$ (the A terms) and the others shifting to the right by the same amount (the B terms), as in Fig. 3. Because there are two substates at each unit cell, the energy splits into two bands, as in section II. Taking into account that the l_{\pm} and u_{\pm} defined in Eq. 14 gain phases $\pm k/4$ from the shifts away from

the cell center, the state then becomes:

$$\begin{aligned} \psi_{k\pm}(r) = & \frac{1}{\sqrt{2N}} \sum_{n=1}^N \left[\left(u_{\pm} e^{ik/4} \right) e^{ik(n-\frac{1}{4})} \phi \left(r - \left(n - \frac{1}{4} \right) \right) \right. \\ & \left. + \left(l_{\pm} e^{-ik/4} \right) e^{ik(n+\frac{1}{4})} \phi \left(r - \left(n + \frac{1}{4} \right) \right) \right] \end{aligned} \quad (21)$$

$$\begin{aligned} = & \frac{1}{\sqrt{2N}} \sum_{n=1}^N e^{ikn} \left[\phi \left(r - n + \frac{1}{4} \right) \right. \\ & \left. \pm e^{-i\theta_k + ik/2} \phi \left(r - n - \frac{1}{4} \right) \right], \end{aligned} \quad (22)$$

where the \pm labels correspond to the two eigenstates in the upper (+) and lower (−) bands. The first Wannier function inside the square bracket is centered at the A subsites, while the second function is localized near the B subsites.

Finally, the main interest here is not in wavefunctions of fixed k , but rather in states that are initially localized in position. Any position-space wavefunction at $t = 0$ can be expanded in terms of energy eigenstates,

$$\psi(r) = \sum_{k=1}^N (A_{k+} \psi_{k+}(r) + A_{k-} \psi_{k-}(r)). \quad (23)$$

The $A_{k\pm}$ coefficients can be found by taking the overlaps between $\psi(r)$ and the known initial wavefunction. There are two possibilities for the initial state: the photon may be inserted at an A subsite or a B subsite. In the first case, we take the initial state to be

$$\psi_A(r) = \phi \left(r - n_0 + \frac{1}{4} \right), \quad (24)$$

with n_0 being the label of the initial lattice site. In the latter case, we take the wavefunction to be

$$\psi_B(r) = \phi \left(r - n_0 - \frac{1}{4} \right), \quad (25)$$

Making use of the orthonormality of the Wannier functions, it is straightforward then to find that the wavefunctions at $t = 0$ for the two cases are

$$\psi_A(r) = \frac{1}{\sqrt{2N}} \sum_k e^{-ikn_0} (\psi_{k+}(r) + \psi_{k-}(r)) \quad (26)$$

$$\begin{aligned} \psi_B(r) = & \frac{1}{\sqrt{2N}} \sum_k e^{-ikn_0} e^{+i(\theta_k - \frac{k}{2})} \\ & \times (\psi_{k+}(r) - \psi_{k-}(r)). \end{aligned} \quad (27)$$

Clearly, the k values are uniformly distributed in probability, as would be expected for a wavefunction localized in space.

Again using the orthonormality of the Wannier functions, it follows readily that these initially-localized functions also form an orthonormal set:

$$\int \psi_A^*(r) \psi'_A(r) dr = \delta(n'_0 - n_0) \quad (28)$$

$$\int \psi_B^*(r) \psi'_B(r) dr = \delta(n'_0 - n_0) \quad (29)$$

$$\int \psi_B^*(r) \psi'_A(r) dr = 0. \quad (30)$$

where n_0 and n'_0 are the initial cells of the two wavefunctions.

All of the expressions above were at $t = 0$. Evolving forward in time, the energy eigenstates become

$$\psi_{k+}(r, t) = e^{-iE_k t} \psi_{k+}(r) \quad (31)$$

$$= \frac{1}{\sqrt{2N}} \sum_{n=1}^N e^{i(kn - E_k t)} \left[\phi\left(r - n + \frac{1}{4}\right) + e^{-i\theta_k + ik/2} \phi\left(r - n - \frac{1}{4}\right) \right] \quad (32)$$

$$\psi_{k-}(r, t) = e^{+iE_k t} \psi_{k-}(r) \quad (33)$$

$$= \frac{1}{\sqrt{2N}} \sum_{n=1}^N e^{i(kn + E_k t)} \left[\phi\left(r - n + \frac{1}{4}\right) - e^{-i\theta_k + ik/2} \phi\left(r - n - \frac{1}{4}\right) \right] \quad (34)$$

This means that the A - and B -type wavefunctions become

$$\psi_A(r, t) = \frac{1}{N} \sum_{kn} e^{ik(n - n_0)} \left(\phi\left(r - n + \frac{1}{4}\right) \cos(E_k t) + i e^{-i\theta_k + ik/2} \phi\left(r - n - \frac{1}{4}\right) \sin(E_k t) \right)$$

$$\psi_B(r, t) = \frac{1}{N} \sum_{kn} e^{ik(n - n_0)} \times \left(i e^{i\theta_k - ik/2} \phi\left(r - n + \frac{1}{4}\right) \sin(E_k t) + \phi\left(r - n - \frac{1}{4}\right) \cos(E_k t) \right) \quad (35)$$

where t is an integer multiple of some discrete time interval T . Time evolution only alters the phase of each k component by a factor $e^{iE(k)t}$, and therefore the probability of finding each k value is constant in time. However interference between different terms in the sum leads to nontrivial time evolution for the spatial distribution.

Note that the factor of $e^{i(kn - E_k t)}$ in Eq. 32, which implies that the states ψ_{k+} on the positive-energy band are right-moving for positive k and left-moving for negative k . The negative-energy states ψ_{k-} move in the opposite direction: left for $k > 0$ and right for $k < 0$.

IV. TOPOLOGICAL TRANSITIONS

Recall that the topological sector of the system is determined by whether $v > w$ or $v < w$. Consider two sets

of values of (v, w) and (v', w') , leading to two values of the phases, θ_k and θ'_k , and corresponding wavefunctions $\psi_{k\pm}(r)$ and $\psi'_{k\pm}(r)$. These wavefunctions are eigenstates of Hamiltonians $\hat{H}(k)$ and $\hat{H}'(k)$. We take the full Hamiltonian of the system to be $H(k)$ for $n = -N + 1, \dots, 0$ and $H'(k)$ for $n = 1, \dots, N$, where N is assumed large enough to ignore effects from the ends.

Now suppose that $\hat{H}(k)$ and $\hat{H}'(k)$ differ in winding number. Among other things, this implies that the signs of θ_k and θ'_k are opposite at the same value of k . We will restrict ourselves to the simplest case and assume that the initial and final hopping amplitudes are simply interchanged: $v' = w$ and $w' = v$. In this case, we find that:

$$\theta'_k = -\theta_k = +\theta_{-k}. \quad (37)$$

Referring to Eq. 22 and suppressing the time-dependent factors for simplicity, the energy eigenstates of H' can be written in terms of the phase θ_k of H as:

$$\psi'_{k\pm}(r) = \frac{1}{\sqrt{2N}} \sum_{n=1}^N e^{ikn} \left[\phi\left(r - n + \frac{1}{4}\right) \pm e^{+i\theta_k - ik/2} \phi\left(r - n - \frac{1}{4}\right) \right] \quad (38)$$

$$= \frac{1}{\sqrt{2N}} \sum_{n=1}^N e^{i(kn + \theta_k + k/2)} \left[e^{-i\theta_k - ik/2} \phi\left(r - n + \frac{1}{4}\right) \pm \phi\left(r - n - \frac{1}{4}\right) \right]. \quad (39)$$

Now shift the origin by $\frac{1}{2}$ unit, $r \rightarrow r - \frac{1}{2}$, and shift the summation index $n \rightarrow n - 1$ in the second sum. After a few steps of algebra, one finds that the new wavefunctions are related to the old ones by:

$$\psi'_{k\pm}(r) = \pm e^{i(\theta_k - \frac{3k}{2})} \psi_{k\pm}(r). \quad (40)$$

The phases linear in k come from the shifts in origin for r and n . The A and B wavefunctions are now:

$$\psi'_A(r) = \frac{1}{\sqrt{2N}} \sum_k e^{-ikn_0} e^{i(\theta_k - \frac{3k}{2})} (\psi_{k+} - \psi_{k-}) \quad (41)$$

$$\psi'_B(r) = \frac{1}{\sqrt{2N}} \sum_k e^{-ik(n_0 + 2)} (\psi_{k+} + \psi_{k-}). \quad (42)$$

Aside from the extra phase factors, it can be seen that the change of winding number as the Hamiltonian changes from H to H' has effectively converted the A -type wavefunctions into B -type wavefunctions, and vice-versa.

The interchange of v and w essentially redefines the unit cells, shifting each cell by one-half unit. This interchanges the roles of the A and B subsites, as shown in Fig. 4. Moreover, as would be expected from a topological transition, the change from A being to the left of B within the unit cell to having A on the right is a *discrete* change, and this change must be carried out globally on the entire system.

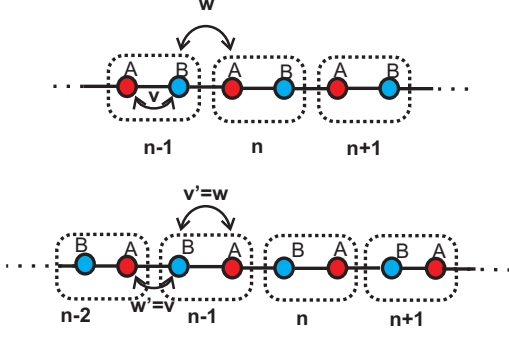


FIG. 4: Interchanging v and w amounts to shifting the units cells by a distance of $\frac{1}{2}$ units, which effectively reverses the roles of A and B subsites. The top and bottom figures represent the two cases.

In the case we consider, $v' = w$ and $w' = v$, it should be noted that the energy eigenvalues are the same on both sides of the boundary: $E_k = E'_k$, so the reflection is not due to any mismatch of energy levels. In fact, the total energy of the A and B modes vanishes on both sides. For example,

$$E_A = \langle \psi_A | \hat{H} | \psi_A \rangle \quad (43)$$

$$= \frac{1}{2N} \sum_{k,k'} e^{-i(k-k')n_0} \quad (44)$$

$$\times [+E_k (\langle \psi_{k'+} | \psi_{k+} \rangle + \langle \psi_{k'-} | \psi_{k+} \rangle) \quad (45)$$

$$- E_k (\langle \psi_{k'+} | \psi_{k-} \rangle + \langle \psi_{k'-} | \psi_{k-} \rangle)] \quad (46)$$

$$= 0. \quad (47)$$

The vanishing of the energies makes intuitive sense: each A or B state is an equal superposition of eigenstates from the upper and lower bands. Since the energies of the two bands are negatives of each other, the total energy must be zero.

A more quantitative examination can be made of the transition across the boundary. We take the boundary to occur at the $n = 0$ cell, with the roles of v and w reversing once the B subsite of that cell is crossed. Only right-moving modes can cross from the left side to the right, so consider a positive-energy right-moving mode ($k > 0$) encountering the boundary; some of the amplitude can reflect to the left, some may be transmitted to the right. In addition, a localized edge state can be built up around the boundary. So one may consider a state of the form

$$|\Psi\rangle = |\psi_{k+}\rangle + r_k |\psi_{-k,+}\rangle + t_k |\psi'_{k+}\rangle + |\psi_{e,k}\rangle, \quad (48)$$

where the terms on the right represent the incident, reflected, transmitted, and edge states. (A similar state can be constructed using a right-moving negative energy state with $k < 0$; the results will be similar.) This state must satisfy the eigenvalue equation

$$\hat{H}|\Psi\rangle = E_k|\Psi\rangle. \quad (49)$$

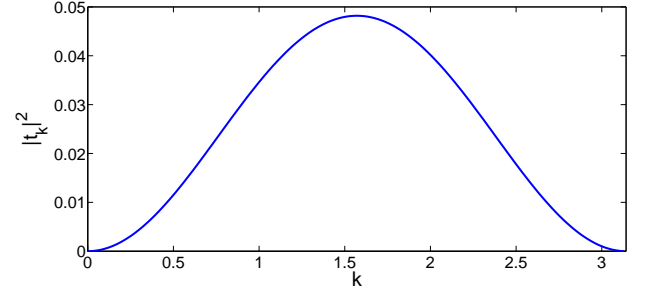


FIG. 5: The transmission probability $|t_k|^2$ between the regions of different winding number always peaks at $k = \frac{\pi}{2}$, dropping to 0 at $k = 0, \pi$. The plot here is for $N = 500$, $v = 0.1$, and $w = 0.9$.

Eq. 49 can be solved exactly: the solutions for a_0 , b_0 , a_1 , b_1 , as well as for the reflection and transmission amplitudes r_k and t_k , are given in the appendix. For given values of v and w , the transmission probability at a fixed k value, $|t_k|$, peaks at $k = \frac{\pi}{2}$, dropping to zero at $k = 0, \pi$ (Fig. 5). When the two hopping amplitudes are equal, $v = w$, the transmission is 100%, as would be expected, since the two sides of the boundary are identical at this value. However, as the difference $|v - w|$ increases, the peak transmission drops (Fig. 6).

We see then that by choosing w close to 0 and v close to 1, or vice versa, we can make the transmission of the wavefunction into the second region arbitrarily small, even though the energy levels are identical on both sides. A figure of merit might be taken to be

$$T_{max} \equiv \max_k (|t_k|^2), \quad (50)$$

the fixed- k transition probability, maximized over all k values. Then, for example, if it is desired to keep $T_{max} \leq 10^{-3}$, this can be accomplished by arranging to have $\left| \frac{v-w}{v+w} \right| > .96$

V. CONCLUSION

In this paper, we have constructed explicit expressions for the position-space wavefunctions of the SSH model in the case of an initially localized particle, and examined what happens to them when the propagating wavefunction encounters a change in system parameters that discontinuously alters the system's winding number. Any modes hitting the interface between regions exhibits some reflection backward. Therefore transmissions across the boundary are suppressed, and if v and w are well-chosen they can be made arbitrarily small. It is well-known that localized edge states existing at boundaries between regions with different values of a topological invariant enjoy a form of protection against perturbations. The results here imply that under some conditions a weaker form of protection can be made to extend to states in the bulk

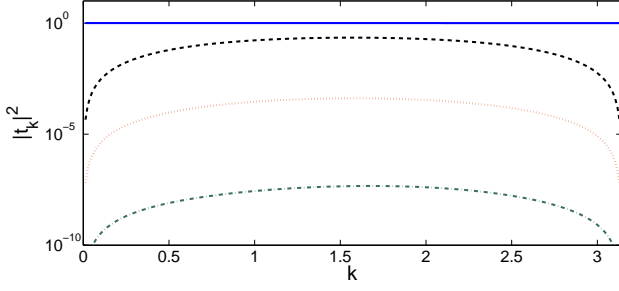


FIG. 6: Logarithmic plot of transmission probability $|t_k|^2$ for several values of v and w . The transmission probability is constant at $|t_k|^2 = 1.0$ for $v = w$, but drops as $|v - w|$ increases. Increasing $|v - w|$ increases the value of $|\theta_k|$ at each nonzero k , leading to a larger phase shift at the boundary. The values plotted here are $(v, w) = (.5, .5)$ (solid blue), $(.2, .8)$ (dashed black), $(.01, .99)$ (dotted red), and $(.001, .999)$ (dash-dot green). As $|v - w| \rightarrow 1$, the peak transmission $|t_k|^2 \rightarrow 0$.

regions: if a severe external perturbation to the Hamiltonian causes a change in winding number in some region, the wavefunction resists entering that region, and tends to stay in the unperturbed region of original winding number. Since this happens due to the change in a topological quantum number, it could be referred to as “topologically-assisted suppression of transitions” of the bulk wavefunction. This effect has obvious applications, since it can be used to protect quantum information encoded in bulk wavefunctions against environment-induced errors. Such applications will be examined in detail elsewhere.

Acknowledgements

This research was supported by the National Science Foundation EFRI-ACQUIRE Grant No. ECCS-1640968, AFOSR Grant No. FA9550-18-1-0056, and by the Northrop Grumman NG Next.

Appendix: Exact Solution of Wavefunction Across Topological Boundary

Consider a right-moving state coming from the left and hitting the boundary between the two regions of different winding number. We will consider only states on the upper energy band; the negative energy band is similar. The full state of the system can be written in the form

$$|\Psi\rangle = |\psi_{k+}\rangle + r_k |\psi_{-k,+}\rangle + t_k |\psi'_{k+}\rangle + |\psi_{e,k}\rangle, \quad (\text{A.1})$$

for $k > 0$ (right-moving incident wave), where the terms on the left represent, respectively, the incident, reflected, and transmitted state, as well as a localized edge state $|\psi_{e,k}\rangle$. We take the boundary to pass through the B subcell of the $n = 0$ site. Referring to Fig. 7, the transition

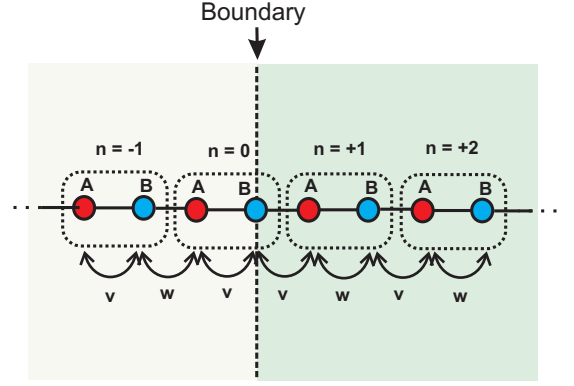


FIG. 7: The boundary between distinct topological regions is taken to pass through the B subcell of site $n = 0$. When the boundary is crossed, the roles of v and w are interchanged.

between the two asymptotic solutions takes place over the span of the $n = 0$ and $n = 1$ sites, so the edge state may be expressed as

$$|\psi_{e,k}\rangle = \frac{1}{\sqrt{2N}} (a_0 |A, 0\rangle + b_0 |B, 0\rangle + a_1 |A, 1\rangle + b_1 |B, 1\rangle). \quad (\text{A.2})$$

Using Eqs. 35 and 36, the state may be written as

$$\begin{aligned} |\Psi\rangle = \frac{1}{\sqrt{2N}} \Bigg\{ & \sum_{n=-N+1}^{-1} \left[e^{ikn} (|A, n\rangle + e^{-i(\theta_k - k/2)} |B, n\rangle) \right. \\ & \left. + r_k e^{-ikn} (|A, n\rangle + e^{i(\theta_k - k/2)} |B, n\rangle) \right] \\ & + t_k \sum_{n=2}^N e^{ikn} (|A, n\rangle + e^{i(\theta_k + k/2)} |B, n\rangle) \\ & \left. + a_0 |A, 0\rangle + b_0 |B, 0\rangle + a_1 |A, 1\rangle + b_1 |B, 1\rangle \right\}. \end{aligned} \quad (\text{A.3})$$

Here, use has been made of the fact that the sign of θ_k changes as the boundary is crossed.

The Hamiltonian is of the form of Eq. 3 to the left of the boundary, while on the right it is of the same form with v and w interchanged. Keeping mind that the interchange of v and w also flips the sign of θ_k , this gives

$$\begin{aligned} \hat{H}|\Psi\rangle = \frac{1}{\sqrt{2N}} \Bigg\{ & \sum_{n=-N+1}^{-1} \left[(e^{ikn} + r_k e^{-ikn}) \right. \\ & \times (v|B, n\rangle + w|B, n-1\rangle) \\ & + (e^{ikn} e^{-i(\theta_k - k/2)} + r_k e^{-ikn} e^{i(\theta_k - k/2)}) \\ & \times (v|A, n\rangle + w|A, n+1\rangle) \Big] \\ & + t_k \sum_{n=2}^N e^{ikn} [(v|B, n-1\rangle + w|B, n\rangle) \\ & + e^{i(\theta_k + k/2)} (v|A, n+1\rangle + w|A, n\rangle)] \\ & + a_0 (v|B, 0\rangle + w|B, -1\rangle) + b_0 (v|A, 0\rangle + v|A, 1\rangle) \\ & \left. + a_1 (v|B, 0\rangle + w|B, 1\rangle) + b_1 (w|A, 1\rangle + v|A, 2\rangle) \right\}. \end{aligned} \quad (\text{A.4})$$

The state must satisfy $\hat{H}|\Psi\rangle = E_k|\Psi\rangle$. Equating terms of the same kind ($|A, 1\rangle$, $|B, 0\rangle$, etc.) on each side leads to a set of equations that can be combined into a matrix equation of the form

$$M \cdot V = W, \quad (\text{A.5})$$

where

$$M = \begin{pmatrix} 0 & v & -E_k & w & 0 & 0 \\ v & -E_k & v & 0 & 0 & 0 \\ 0 & 0 & w & -E_k & 0 & vy^4 \\ -E_k & v & 0 & 0 & \frac{wy}{x} & 0 \\ w & 0 & 0 & 0 & y(yv - \frac{E_k}{x}) & 0 \\ 0 & 0 & 0 & \frac{v}{y^2} & 0 & y(\frac{wy^2}{x} - E_k y) \end{pmatrix} \quad (\text{A.6})$$

and

$$V = \begin{pmatrix} a_0 \\ b_0 \\ a_1 \\ b_1 \\ r_k \\ t_k \end{pmatrix}, \quad W = \begin{pmatrix} 0 \\ 0 \\ 0 \\ -wx/y \\ \frac{(E_k x - v/y)y}{y} \\ 0 \end{pmatrix}. \quad (\text{A.7})$$

Here, we have defined $x = e^{-i\theta_k}$ and $y = e^{ik/2}$. Making the further definition

$$D^{-1} = y^2((E^6 - v^4 w^2 + E^2(v^2 + w^2)(2v^2 + w^2) - E^4(3v^2 + 2w^2))x + (E^2 - v^2)vx^2)y - E(E^2 - 2v^2 - w^2)((E^2 - w^2)w + vw(E^4 + v^2 w^2 - E^2(2v^2 + w^2))xy^2), \quad (\text{A.8})$$

then the solutions of these equations are given by

$$a_0 = -D(vw((E_k^4 + v^4 - E_k^2(2v^2 + w^2))x + E_k w(-E_k^2 + v^2 + w^2)y)(x^2 y^2 - 1)) \quad (\text{A.9})$$

$$b_0 = D(v^2 w(-E_k^3 x + E_k(v^2 + w^2)x + E_k^2 w y - w^3 y)(x^2 y^2 - 1)) \quad (\text{A.10})$$

$$a_1 = D(v^3 w(-E_k^2 x + v^2 x + E_k w y)(x^2 y^2 - 1)) \quad (\text{A.11})$$

$$b_1 = D(v^3 w^2(-E_k x + w y)(x^2 y^2 - 1)) \quad (\text{A.12})$$

$$r_k = Dy^{-1}(x(E_k v(v^2 - E_k^2)(-E_k^2 + 2v^2 + w^2)x - (E_k^6 x^2 + v^3 w^2(w - vx^2) + E_k^2(2v^2 + w^2)(-vw + (v^2 + w^2)x^2) + E_k^4(vw - (3v^2 + 2w^2)x^2))y + E_k w(E_k^2 - w^2)(E_k^2 - 2v^2 - w^2)xy^2)) \quad (\text{A.13})$$

$$t_k = Dy^{-4}(v^4 w^2 x(1 - x^2 y^2)). \quad (\text{A.14})$$

Substituting these formulas into Eqs. A.1-A.2 gives an exact solution to the eigenvalue problem. The reflection and transmission coefficients of Eqs. A.13 and A.14 were used to construct the plots of Figs. 5 and 6.

-
- [1] W. P. Su, J. R. Schrieffer, and A. J. Heeger, *Phys. Rev. B* **22**, 2099 (1980).
 - [2] M. Z. Hasan, C. L. Kane, *Rev. Mod. Phys.* **82**, 3045 (2010)
 - [3] J. K. Asbóth, L. Oroszlány, A. P. Pályi, *A Short Course on Topological Insulators: Band Structure and Edge States in One and Two Dimensions* (Springer, Heidelberg, 2017)
 - [4] T. Kitagawa, M. S. Rudner, E. Berg, and E. Demler, *Phys. Rev. A* **82**, 033429 (2010)
 - [5] M. A. Broome, A. Fedrizzi, B. P. Lanyon, I. Kassal, A. Aspuru-Guzik, A. G. White, *Phys. Rev. Lett.* **104**, 153602 (2010)
 - [6] T. Kitagawa, M. S. Rudner, E. Berg, E. Demler, *Phys. Rev. A* **82**, 033429 (2010)
 - [7] T. Kitagawa, E. Berg, M. Rudner, and E. Demler, *Phys. Rev. B* **82**, 235114 (2010)
 - [8] T. Kitagawa, M. A. Broome, A. Fedrizzi, M. S. Rudner, E. Berg, I. Kassal, A. Aspuru-Guzik, E. Demler, and A. G. White, *Nature Comm.* **3**, 882 (2012)
 - [9] B. Tarasinski, J. K. Asbóth, and J. P. Dahlhaus, *Phys. Rev. A* **89**, 042327 (2014)
 - [10] F. Cardano, A. D'Errico, A. Dauphin, M. Maffei, B. Piccirillo, C. de Lisio, G. De Filippis, V. Cataudella, E. Santamato, L. Marrucci, M. Lewenstein, P. Massignan, *Nat. Comm.* **8**, 15516 (2017)
 - [11] D. S. Simon, C. A. Fitzpatrick, S. Osawa, and A. V. Sergienko, *Phys. Rev. A* **96**, 013858 (2017)
 - [12] D. S. Simon, C. A. Fitzpatrick, S. Osawa, and A. V. Sergienko, *Phys. Rev. A* **95**, 042109 (2017)
 - [13] J. Kempe, *Contemp. Phys.* **44**, 307 (2003)
 - [14] A. Ambainis, *Int. J. Quant. Inf.* **1**, 507 (2003)
 - [15] R. Portugal, *Quantum Walks and Search Algorithms* (Springer, Berlin, 2013)
 - [16] R. Jackiw and C. Rebbi, *Phys. Rev. D* **13**, 3398 (1976).
 - [17] G. H. Wannier, *Phys. Rev.* **52**, 191 (1937).
 - [18] W. Kohn, *Phys. Rev.* **115**, 809 (1959).
 - [19] J. des Cloizeaux, *Phys. Rev.* **129**, 554 (1963).